Evaluation of Oxide Layer Thickness (ZnO, Al_2O_3, $BaTiO_3$, TiO_2) as an Interlayer and Sensitive Layer in SPR Sensors

Freygieon Ogiek Rizal Sukma[1*], I Made Satriya Wibawa[1], Hangga Novian Adi Putra[1], Putu Gede Agus Krisna Yogantara[1]

[1]Department of Physics, Faculty of Mathematics and Natural Sciences, Universitas Udayana, Bali, Indonesia

Email: *ogiek@unud.ac.id; satriya_wibawa@unud.ac.id; hangga@unud.ac.id; krisna_yogantara@unud.ac.id

Received: 16th January 2026; Revised: 8th February 2026; Accepted: 8th February 2026

Abstract –. *Numerical simulation of a Surface Plasmon Resonance (SPR) sensor was carried out using COMSOL Multiphysics 5.5 based on the Finite Element Method (FEM) to evaluate detection performance influenced by oxide type and thickness acting as interlayer and sensitive layer. The sensor configuration employs silver (Ag) as the plasmonic metal, while ZnO, Al_2O_3, $BaTiO_3$, and TiO_2 are considered as oxide materials. The presence of an oxide layer with a certain thickness gives different resonance curve characteristics due to changes in the resulting plasmonic coupling. In this study, $BaTiO_3$ with a thickness of 40 nm obtained the optimum condition with a minimum FWHM value, accompanied by high FOM value of around 107.75 RIU^{-1}. Meanwhile, the use of oxide materials as sensitive layers causes a shift of the resonance angle toward higher values with increasing refractive index and thickness, resulting in enhanced angular sensitivity. However, this improvement is accompanied by a broadening of the FWHM, indicating increased plasmon damping associated with the sensitive layer. Among the evaluated configurations, the $BaTiO_3$ (40 nm)/Ag (50 nm)/Al_2O_3 (10 nm) structure exhibits the lowest minimum reflectance and a FOM of 91.35 RIU^{-1}. Despite a marginal reduction in the FOM, the sensitivity attains about 150°/RIU, exceeding that of the configuration without a sensitive layer (120°/RIU). Field profile reveals reduced penetration depth, indicating surface-confined electromagnetic fields beneficial for gas sensing. This study provides insight into the dual role of oxide layers as interlayers and sensitive layers for optimizing electromagnetic confinement, sensitivity, and design strategy for SPR-based gas sensing platforms.*

Keywords: *SPR; Performance; Ag; Oxide Layer; FEM.*

1. Introduction

The resonance condition due to the matching of the momentum between the incident light and the oscillation of free electrons at the metal-dielectric interface, known as the SPR phenomenon, has been developed and studied for its application as an optical sensor for several decades [1]. The matching of the momentum is realized using the Kretschmann configuration, which consists of a glass with a high refractive index (prism) coated with a thin metal layer [2]. In the resonance condition, the decrease in reflectance intensity in the TIR condition occurs due to the excitation of surface plasmons at the prism-air interface. This resonance condition is very sensitive to changes in the refractive index of the medium around the metal surface, so that this principle is utilized as a detection mechanism. In the SPR sensor, the analyte response is detected through the shift in the resonance angle, namely the angle at which the minimum reflectance occurs, which is caused by changes in the refractive index of the sensing medium (air) at the metal surface due to the presence of the analyte [3].

SPR sensors have been extensively investigated for various detection applications because they offer real-time monitoring capabilities and high sensitivity [4]. Advances in fabrication technology in recent years have improved the performance of SPR sensors based on the Kretschmann configuration, particularly in terms of sensitivity and resonance coupling efficiency. One widely developed approach is the integration of oxide materials into the SPR sensor structure.

Oxide materials in SPR sensors have been reported to function as sensitive layers, considering that oxide layers exhibit specific interactions with gas molecules and have been widely applied as sensitive

layers in various non-SPR gas sensors [5,6]. In SPR sensors, the presence of an oxide layer on the metal surface as a sensitive layer not only enhances analyte sensitivity through improved selectivity but also increases sensor sensitivity due to an increase in the effective refractive index of the surrounding air medium near the metal surface, given that oxide materials generally possess relatively high refractive indices [7–10]. In addition to serving as sensitive layers, several studies have also reported the use of oxide materials as interlayers between the prism and the metal layer.

One of the key parameters that strongly influences the role of oxide layers in SPR sensors is their thickness. In several theoretical studies, oxide layers have been used as interlayers with varying material types and thicknesses, including ZnO interlayers with thicknesses of around 5 nm [11] and about 40 nm [12], as well as TiO_2 interlayers of approximately 10 nm [13]. However, the specific influence of oxide layers as interlayers, particularly their thickness, remains insufficiently discussed, as most studies primarily report only the overall performance of the sensor structures. A similar situation is observed for oxides functioning as sensitive layers, such as TiO_2 [14], ZnO [15], $BaTiO_3$ [4] , and Al_2O_3 [16], which have also been reported in previous works. Therefore, evaluating the thickness of oxide layers is an important aspect in the design and optimization of SPR sensors. This study aims to investigate the effect of oxide layer thickness when functioning as both an interlayer and a sensitive layer on the SPR resonance characteristics. The results of this study are expected to provide a more comprehensive understanding of the relationship between oxide layer thickness and sensor performance, as well as serve as a reference for the development of more optimal SPR sensor structures.

2. Sensor Design and Numerical Modelling

The SPR scheme of the multilayer structure in this study is shown in Figure 1. The configuration used is the Kretschmann configuration with a thin layer of Ag (50 nm) and four types of oxide materials, namely ZnO, Al_2O_3, $BaTiO_3$ and TiO_2. The dispersive behavior of the materials was incorporated using literature-reported refractive index values at the fixed operating wavelength of 633 nm, as listed in Table 1.

Ag was chosen as the plasmonic metal in this study because it exhibits higher accuracy and superior quality figures compared to Au, which is more commonly used in SPR sensors [17]. An Ag thickness of 50 nm was selected because this thickness generally produces a well-defined SPR dip while maintaining efficient plasmon coupling [18]. Although Ag is less chemically stable than Au, the oxide layer on the Ag surface acts as a protective layer, thereby enhancing its chemical stability. In addition to being deposited on the Ag surface as a sensitive layer, the oxide materials are also employed as interlayers, as illustrated in Figure 1. The effect of oxide layer thickness on the SPR sensor response is systematically evaluated.

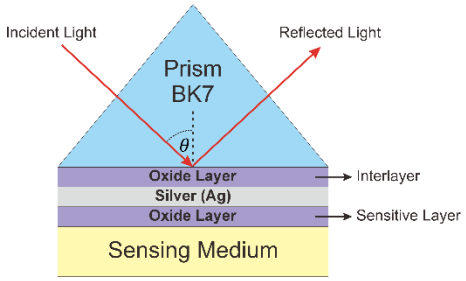

Figure 1. Schematic of the SPR sensor configuration.

Table 1. Complex refractive index of materials at 633 nm.

Material	Refractive Index (n + ik)	Ref.
Prisma BK7	1.515	[13]
Ag	0.0803 + i4.234	[10]
ZnO	1.6248	[15]
Al_2O_3	1.7659	[10]
$BaTiO_3$	2.4043	[4]
TiO_2	2.5837	[19]

The sensor response is observed based on angular modulation. Meanwhile, sensor performance is evaluated through sensitivity (S), detection accuracy (DA), and figure of merit (FOM), defined by the following equations [4]:

$$S = \frac{\delta\theta}{\delta n} \tag{1}$$

$$DA = \frac{1}{FWHM}\ (degree^{-1}) \tag{2}$$

$$FOM = \frac{S}{FWHM}\ (RIU^{-1}) \tag{3}$$

Here, δθ represents the shift in the resonance angle and δn denotes the refractive index change of the analyte, while FWHM corresponds to the full width at half maximum of the absorption peak of the SPR resonance curve.

Numerical analysis of the sensor structure is carried out using the Finite Element Method (FEM). Simulations are performed using COMSOL Multiphysics version 5.5 with a two-dimensional (2D) geometric approach, as shown in Figure 2. The physics model employed is Electromagnetic Waves, Frequency Domain. Periodic port boundary conditions are applied at the top side as the input port (Port 1) and at the bottom side as the output port (Port 2), indicated by blue lines in the figure. Floquet periodic boundary conditions are applied to the lateral sides of the structure, with the wave vector (k-vector) derived from the periodic ports. The mesh structure shown in Figure 2 was generated using an automatic physics-controlled mesh with a finer setting. This meshing approach automatically refines the mesh in regions with high electromagnetic field gradients, ensuring numerical stability, accuracy, and convergence of the simulation results. The wavelength of the light source is set to 633 nm with transverse magnetic (TM) polarization. A wavelength-domain study is conducted with an incident angle sweep from 40° to 80° in increments of 0.1°. The sensing medium is assigned a refractive index of 1.330, and a refractive index of 1.335 is considered to represent variations caused by the analyte.

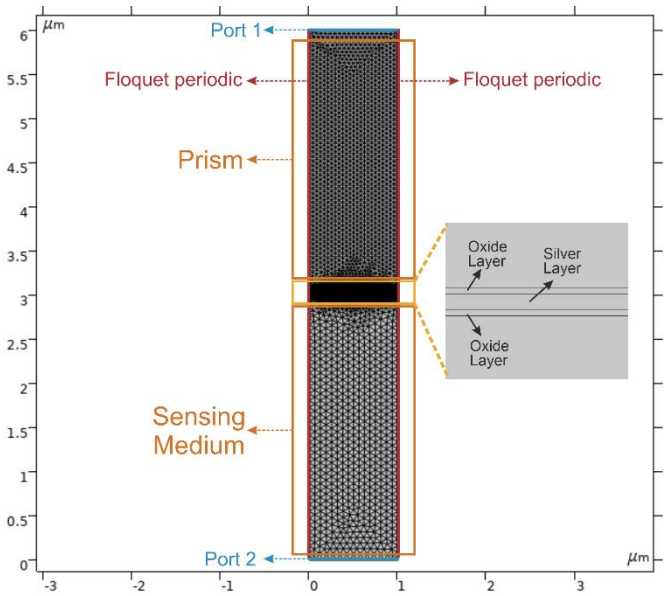

Figure 2. Schematic of the two-dimensional FEM-based SPR sensor simulation model implemented in COMSOL Multiphysics.

3. Result and Discussion

3.1 Analysis of the Effects of Interlayer Thickness and Oxide Type on SPR Curves

The initial optimization was performed on the interlayer thickness of the SPR sensor structure using TiO_2 as the interlayer, as shown in Figure 3(a). The presence of the oxide layer produces SPR curve

characteristics that differ from those of the Ag structure without an interlayer, indicating a change in plasmon coupling conditions [11]. Based on Table 2, the incorporation of TiO_2 as an interlayer causes a shift in the resonance angle (θ_1) from 67.65° for the Ag-only structure to 67.70–67.80° for structures with an interlayer. The resonance angle shift begins to appear at a thickness of 40 nm, increasing from 67.65° to 67.70°, and further increases to 67.75° at thicknesses of 50–60 nm. However, at thicknesses of 70–100 nm, the resonance angle remains at 67.80° without significant change. In terms of FWHM, the Ag structure without an interlayer exhibits an FWHM of 1.318°. The addition of TiO_2 with thicknesses ranging from 10 to 40 nm results in a gradual decrease in FWHM, reaching a minimum value of 1.135° at a thickness of 40 nm. This indicates an improvement in the sharpness of the SPR curve at this thickness. However, for thicknesses greater than 40 nm, the FWHM value increases again, reaching 1.508° at a thickness of 100 nm. This phenomenon occurs because the TiO_2 interlayer has a higher refractive index than the prism, which increases the parallel momentum component of the evanescent wave and leads to improved momentum-matching conditions, thereby shifting the resonance angle toward higher angles [20].

At a certain thickness (around 40 nm), the contribution of TiO_2 and the phase of the evanescent field reach a condition of minimum plasmon damping because the imaginary part of the surface plasmon polariton wave vector, $Im(k_{spp})$, attains its minimum value, resulting in the narrowest FWHM [21]. In contrast, at larger interlayer thicknesses, phase shifts of the electromagnetic field and an increase in the effective refractive index lead to phase mismatch. Consequently, the electromagnetic field becomes less localized at the metal–oxide interface and the damping increases again, as indicated by the broadening of the FWHM. Meanwhile, the minimum reflectance value also exhibits fluctuating behavior with respect to interlayer thickness. Nevertheless, for thicknesses in the range of 10–90 nm, the minimum reflectance remains below 1%, indicating that plasmon coupling still occurs efficiently. However, at a thickness of 100 nm, the minimum reflectance increases to 1.47%, indicating a reduction in coupling efficiency, such that part of the energy is not coupled into the plasmon mode and is instead reflected.

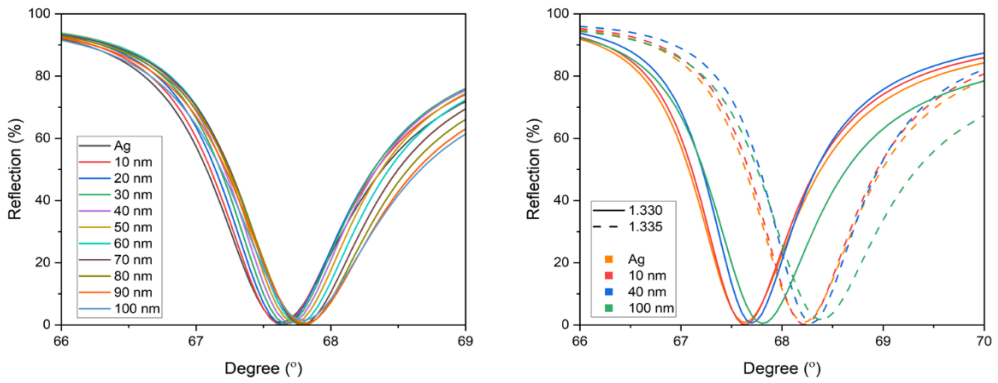

Figure 3. (a) SPR curves for TiO_2 interlayers with different thicknesses, (b) resonance angle shifts at selected interlayer thicknesses.

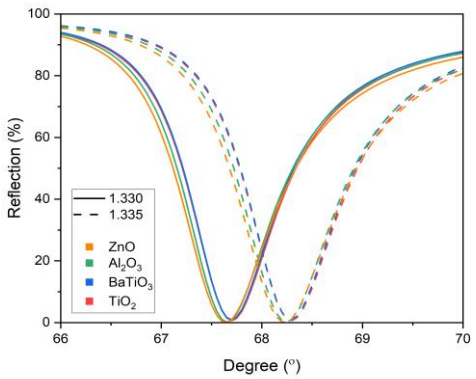

Figure 4. SPR curves with different oxide interlayers.

Based on the combination of the smallest FWHM (1.135°) and a sufficiently low minimum reflectance, the optimum thickness of TiO_2 as an interlayer is determined to be 40 nm. To evaluate sensor performance, simulations were carried out by varying the refractive index of the sensing medium from 1.330 to 1.335, and the results are summarized in Table 3. The Ag structure without an interlayer exhibits a sensitivity of 110 °/RIU with a FOM of 83.44 RIU^{-1}. The addition of TiO_2 improves the sensor performance, where TiO_2 with a thickness of 40 nm yields a sensitivity of 120 °/RIU and the highest FOM of 105.73 RIU^{-1} compared to other thicknesses. In contrast, although TiO_2 with a thickness of 100 nm shows the same sensitivity (120 °/RIU), its FOM decreases to 79.56 RIU^{-1} due to the increased FWHM.

Subsequently, the effect of oxide type was investigated by employing interlayers with a fixed thickness of 40 nm, namely $BaTiO_3$, Al_2O_3, and ZnO. Based on Table 2, $BaTiO_3$ exhibits the smallest FWHM (1.114° at 40 nm) compared to the other oxides, while Table 3 shows that $BaTiO_3$ also provides the highest FOM of 107.75 RIU^{-1}. This indicates that $BaTiO_3$ is capable of producing a sharper SPR curve and superior sensor performance. To confirm the consistency of the optimum thickness, $BaTiO_3$ was also analyzed at thicknesses of 30 and 50 nm. The results show that a thickness of 40 nm still yields the smallest FWHM compared to the other thicknesses, indicating that 40 nm is the optimum thickness for both TiO_2 and $BaTiO_3$ as interlayers. Differences in oxide materials, which represent differences in interlayer refractive indices, result in different plasmon coupling conditions. At a given operating wavelength, an interlayer with an excessively high refractive index can cause over-confinement of the electromagnetic field within the interlayer, thereby reducing the interaction between the field and the sensing medium. In this configuration, $BaTiO_3$ with a thickness of 40 nm achieves an optimal momentum-matching condition, resulting in a sharper SPR curve and a higher FOM value.

Table 2. SPR curve characteristics with interlayers at various thicknesses (n = 1.330).

Interlayer	Thickness (nm)	FWHM (°)	Reflectance (%)	θ_1 (°)
Ag (without interlayer)	–	1.318	0.91	67.65
TiO_2	10	1.231	0.17	67.65
TiO_2	20	1.173	0.04	67.65
TiO_2	30	1.144	0.53	67.65
TiO_2	40	1.135	0.64	67.70
TiO_2	50	1.152	0.79	67.75
TiO_2	60	1.190	0.46	67.75
TiO_2	70	1.250	0.17	67.80
TiO_2	80	1.332	0.02	67.80
TiO_2	90	1.426	0.50	67.80
TiO_2	100	1.508	1.47	67.80
$BaTiO_3$	30	1.131	0.61	67.65
$BaTiO_3$	40	1.114	0.93	67.70
$BaTiO_3$	50	1.120	1.35	67.75
Al_2O_3	40	1.152	0.17	67.65
ZnO	40	1.221	0.07	67.65

Table 3. Performance of SPR Sensors with Interlayers.

Interlayer	Thickness (nm)	Accuracy ($°^{-1}$)	Sensitivity (°/RIU)	FOM (RIU^{-1})
Ag (without interlayer)	–	0.758	110	83.44
TiO_2	10	0.812	110	89.33
TiO_2	40	0.881	120	105.73
TiO_2	100	0.663	120	79.56
$BaTiO_3$	40	0.897	120	107.75
Al_2O_3	40	0.868	120	104.17
ZnO	40	0.819	120	98.29

3.2 Analysis of the Effects of Sensitive layer Thickness and Oxide Type on SPR Curves

Figure 5(a) shows the SPR curves for various oxides used as sensitive layers with a thickness of 10 nm on top of a sensor structure that has been optimized using a 40 nm $BaTiO_3$ interlayer. Differences in the type of oxide used as the sensitive layer directly represent differences in the refractive index of the sensitive layer, which in turn modify the effective refractive index in the sensing medium region [22]. As shown in Figure 5(a), an increase in the refractive index of the sensitive layer causes the resonance angle to shift toward higher angles, from approximately 70.40° for ZnO to as high as 80.05° for TiO_2. In terms of curve sharpness, sensitive layers with lower refractive indices, such as ZnO (10 nm), produce the smallest FWHM value (1.446°) along with a relatively low minimum reflectance (2.67%), indicating a sharper resonance. In contrast, sensitive layers with high refractive indices, such as TiO_2, result in much broader SPR curves (FWHM = 3.813°) accompanied by an increase in minimum reflectance to 20.52%. This behavior indicates increased plasmon damping associated with the high-refractive-index sensitive layer, which modifies the electromagnetic field distribution near the sensing interface and leads to degradation of the SPR resonance quality [23]. Nevertheless, an increase in the refractive index of the sensitive layer also leads to an enhancement in angular sensitivity. As summarized in Table 4, the sensitivity increases progressively from 130 °/RIU for ZnO to as high as 300 °/RIU for TiO_2. The shift of the resonance angle toward higher angles at a sensing medium refractive index of n = 1.330 is induced by the presence of the oxide layer, which increases the effective refractive index of the sensing medium. Consequently, this higher resonance angle results in a larger angular shift when the refractive index of the medium changes to n = 1.335 [7].

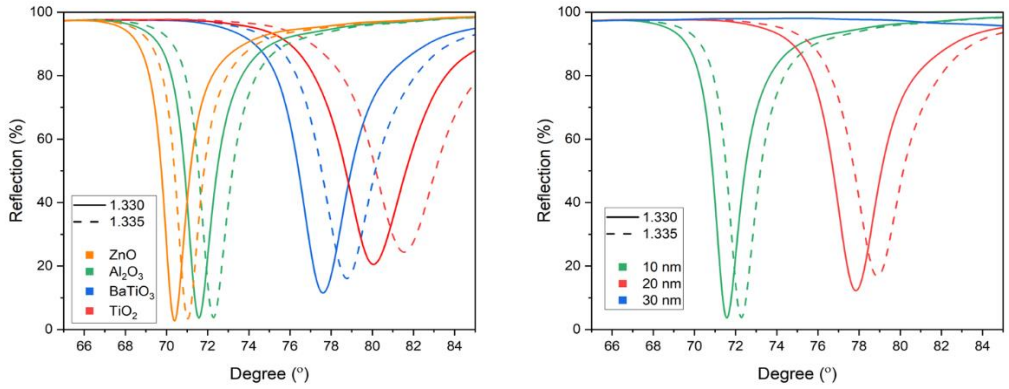

Figure 5. (a) SPR curves of various oxide sensitive layers with a 40 nm $BaTiO_3$ interlayer, (b) effect of Al_2O_3 sensitive layer thickness on SPR curves.

Table 4. Performance of SPR sensors with a $BaTiO_3$ interlayer and various oxide layers as sensitive layers.

Sensitive layer	FWHM (°)	Reflectance (%)	θ_1 (°)	Sensitivity (°/RIU)	FOM (RIU^{-1})
ZnO (10 nm)	1.446	2.67	70.40	130	89.92
Al_2O_3 (10 nm)	1.642	3.72	71.55	150	91.35
Al_2O_3 (20 nm)	2.693	12.24	77.85	210	77.99
$BaTiO_3$ (10 nm)	2.890	11.53	77.60	230	79.57
TiO_2 (10 nm)	3.813	20.52	80.05	300	78.67

Sensor performance is not determined solely by sensitivity, but also by the FOM, which takes into account the width of the resonance curve (Eq. 3). In practical sensing applications using oxide layers as sensitive materials for gas, humidity, and temperature sensing, the refractive index changes are typically small and gradual. Under these conditions, a broad resonance curve can obscure subtle resonance shifts, even when the nominal sensitivity is relatively high. Therefore, the 10 nm Al_2O_3 layer provides a more favorable sensing performance, as its narrower resonance curve results in a higher FOM and enables more precise detection of small refractive index variations.

Based on Table 4, the highest FOM is obtained for Al_2O_3 (10 nm) with an FOM of 91.35 RIU^{-1}, even though its sensitivity (150 °/RIU) is lower than that of $BaTiO_3$ and TiO_2. Figure 5(b) illustrates the effect

of Al_2O_3 sensitive layer thickness on the SPR curve characteristics. Increasing the thickness from 10 nm to 20 nm results in a significant shift of the resonance angle from 71.55° to 77.85°, accompanied by a drastic increase in FWHM from 1.642° to 2.693° and an increase in minimum reflectance from 3.72% to 12.24%. This phenomenon indicates that a thicker sensitive layer enhances the contribution of the sensitive layer refractive index to the effective refractive index of the system, while simultaneously reducing the confinement of the electromagnetic field at the metal–dielectric interface. At a thickness of 30 nm, the SPR phenomenon is no longer observed in the reflectance curve, indicating that the plasmon coupling process is hindered due to excessive damping of the evanescent field.

3.3 Electric field probe profile

Figure 6(a) shows the $BaTiO_3$ (40 nm)/Ag (50 nm)/Al_2O_3 (10 nm) layered structure, where the electromagnetic field is strongly confined around the metal–sensitive layer interface under resonance conditions. This confinement indicates the excitation of Surface Plasmon Polaritons (SPPs). The field distribution with positive and negative amplitudes (red and blue) reflects the oscillatory nature of plasmonic modes bound to the interface. Meanwhile, the electric field profile in Figure 6(b) clearly shows the difference between the non-resonant angle (70°) and the resonance angle (71.55°). At the resonance angle, the electric field is significantly enhanced near the interface and then decays exponentially toward the sensing medium [24]. This strongly localized field in the sensing medium enhances the optical interaction with the analyte, thereby directly contributing to the sensor sensitivity. For the optimum configuration in this study, the penetration depth of the field under resonance conditions, defined as 1/e of the maximum field amplitude [13] is approximately 207.1 nm from the Al_2O_3 surface into the sensing medium. This value is smaller than those obtained for the $BaTiO_3$/Ag (226.6 nm) and Ag-only (228.6 nm) configurations.

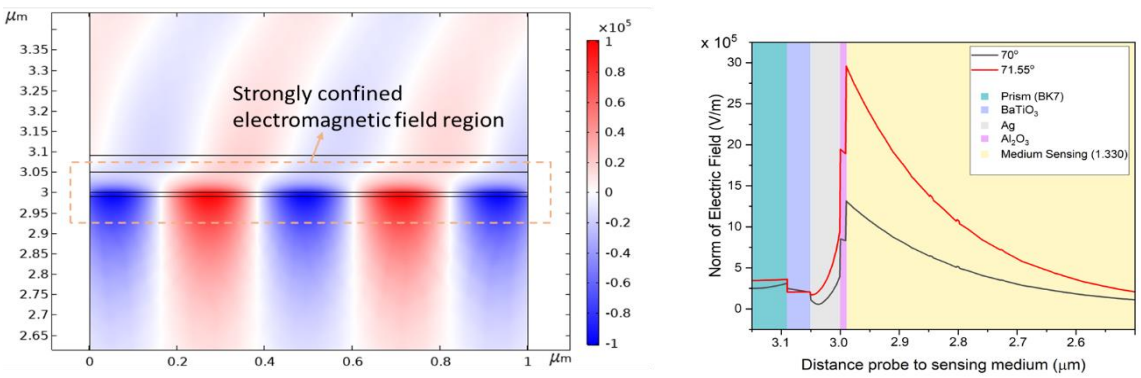

a) b)

Figure 6. (a) Confined electromagnetic field at resonance (71.55°), (b) Electric field norm profile versus distance toward the sensing medium at different incident angles.

The reduced penetration depth indicates stronger spatial confinement of the electromagnetic field near the sensing surface, which can enhance surface sensitivity. However, the broader FWHM observed for higher-refractive-index sensitive layers suggests increased plasmon damping, indicating that field confinement and resonance sharpness do not necessarily vary proportionally in SPR structures incorporating sensitive layers. In addition, this improvement in sensitivity involves a trade-off, as a shallower penetration depth reduces the effective detection volume. Nevertheless, for gas-sensing applications, where detection is primarily governed by adsorption-induced changes at the sensing surface rather than bulk refractive index variations, a more surface-confined electromagnetic field is generally advantageous. Therefore, the oxide-based multilayer configuration employed in this study shows strong potential for gas-sensing applications.

4. Conclusion

Optimization of the thickness and selection of oxide material as an interlayer and sensitive layer affect the resonance conditions, thus affecting the detection performance of the SPR sensor. Oxides used as a

sensitive layer increase sensor sensitivity, but are generally accompanied by a widening of the FWHM. The increase in sensitivity and widening of the FWHM by the presence of oxide as a sensitive layer increases with the increase in the refractive index of the material and the thickness used. Meanwhile, oxides used as an interlayer at a certain thickness and refractive index are able to produce a narrowing of the FWHM, which means increasing sensor accuracy even accompanied by sensitivity that makes the FOM high. In this study, the optimum interlayer thickness was obtained at 40 nm, with $BaTiO_3$ showing the best performance through the smallest FWHM and the highest FOM. Among the configurations studied, the structure of $BaTiO_3$ (40 nm)/Ag (50 nm)/Al_2O_3 (10 nm) provides the best balance between sensitivity and resonance quality, accompanied by a low minimum reflectance value (<10%) and strong electric field confinement with a penetration depth of around 207.1 nm. These results confirm that the performance of the SPR sensor can be improved by optimizing the multilayer structure based on the use of oxide as an interlayer and sensitive layer. Since this study is based on numerical simulations assuming uniform material conditions and optimized parameters, experimental validation is necessary as future work.

Acknowledgment

The author acknowledges Ismawati for the translation assistance that contributed to the smooth completion of this work.

References

[1] Sukma F O R, Hanif M A, Masruroh, Santjojo D J D H, Apsari R, Susanto H and Tazi I 2024 Effects of thickness and roughness on plasmonic characteristics of gold thin films deposited on polished optical fiber *Mater. Res. Express* **11** 016201

[2] Uwais M, Bijalwan A and Rastogi V 2024 SPR-Based Sensor for Colorectal Cancer Detection using Al–Cu and Graphene *Plasmonics* **19** 1857–66

[3] Zhou S, Li J, Zhang Q, Tong Y, Qi X, Duan Y, Zhang X, Luo Z and Li Y 2024 Recent advance on fiber optic SPR/LSPR-based ultra-sensitive biosensors using novel structures and emerging signal amplification strategies *Optics & Laser Technology* **175** 110783

[4] Muthumanikkam M, Vibisha A, Lordwin Prabhakar M C, Suresh P, Rajesh K B, Jaroszewicz Z and Jha R 2023 Numerical Investigation on High-Performance Cu-Based Surface Plasmon Resonance Sensor for Biosensing Application *Sensors* **23** 7495

[5] Kang Y, Yu F, Zhang L, Wang W, Chen L and Li Y 2021 Review of ZnO-based nanomaterials in gas sensors *Solid State Ionics* **360** 115544

[6] Tian X, Cui X, Lai T, Ren J, Yang Z, Xiao M, Wang B, Xiao X and Wang Y 2021 Gas sensors based on TiO2 nanostructured materials for the detection of hazardous gases: A review *Nano Materials Science* **3** 390–403

[7] Prasanth A, Harini V K, Manivannan P, Narasimman S, Velumani M, Meher S R and Alex Z C 2024 A comparative study of ZnO, AZO, TiO2, Sb2O3, and SnO2 nanomaterials coated SPR based fiber optic refractive index sensors for chemical sensing application *Optical Materials* **152** 115438

[8] Sassi I, Rhouma M B E H, Zbidi M and Simatupang J W 2024 A Highly Sensitive Structure Based on Prism, Silver, and Titanium Dioxide for Biochemical Sensing Applications *Plasmonics* **20** 363–72

[9] Karki B, Trabelsi Y, Pal A, Taya S A and Yadav R B 2024 Direct detection of dopamine using zinc oxide nanowire-based surface plasmon resonance sensor *Optical Materials* **147** 114555

[10] Shivangani, Alotaibi M F, Al-Hadeethi Y, Lohia P, Singh S, Dwivedi D K, Umar A, Alzayed H M, Algadi H and Baskoutas S 2022 Numerical Study to Enhance the Sensitivity of a Surface Plasmon Resonance Sensor with BlueP/WS2-Covered Al2O3-Nickel Nanofilms *Nanomaterials* **12** 2205

[11] Janze E J T, Alaei S and Meshginqalam B 2025 On the sensing performance improvement in SPR biosensor using ZnO and TMDCs architecture for cancer detection *Sci Rep* **15** 28349

[12] Mudgal N, Saharia A, Agarwal A and Singh G 2023 ZnO and Bi-metallic (Ag–Au) Layers Based Surface Plasmon Resonance (SPR) Biosensor with $BaTiO_3$ and Graphene for Biosensing Applications *IETE Journal of Research* **69** 932–9

[13] Mostufa S, Akib T B A, Rana Md M and Islam Md R 2022 Highly Sensitive TiO2/Au/Graphene Layer-Based Surface Plasmon Resonance Biosensor for Cancer Detection *Biosensors* **12** 603

[14] El-Gohary S, Choi M, Kim Y and Byun K 2016 Dispersion Curve Engineering of TiO2/Silver Hybrid Substrates for Enhanced Surface Plasmon Resonance Detection *Sensors* **16** 1442

[15] Mustaffa S N, Md Yatim N, Abdul Rashid A R, Pithaih V, Sha'ari N S, Muhammad A R, Abdul Rahman A, Jamil N A and Menon P S 2023 Visible and angular interrogation of Kretschmann-based SPR using hybrid Au–ZnO optical sensor for hyperuricemia detection *Heliyon* **9** e22926

[16] Nur J N, Hasib M H H, Asrafy F, Shushama K N, Inum R and Rana Md M 2019 Improvement of the performance parameters of the surface plasmon resonance biosensor using Al2O3 and WS2 *Opt Quant Electron* **51** 174
[17] Jain S, Paliwal A, Gupta V and Tomar M 2020 SPR studies on optical fiber coated with different plasmonic metals for fabrication of efficient biosensors *Materials Today: Proceedings* **33** 2180–6
[18] Wang Q, Cao S, Gao X, Chen X and Zhang D 2021 Improving the Detection Accuracy of an Ag/Au Bimetallic Surface Plasmon Resonance Biosensor Based on Graphene *Chemosensors* **10** 10
[19] Hossain Md B, Rahman Khan M M, Sadiqur Rahman Md, Bin Badrudduza S S, Sabiha M M and Rana Md M 2019 Graphene-MoS2-Au-TiO2-SiO2 Hybrid SPR Biosensor: A New Window for Formalin Detection *J. Mater. Appl.* **8** 51–8
[20] Chauhan M and Kumar Singh V 2021 Review on recent experimental SPR/LSPR based fiber optic analyte sensors *Optical Fiber Technology* **64** 102580
[21] Kuryoz P Yu, Poperenko L V and Kravets V G 2013 Correlation between dielectric constants and enhancement of surface plasmon resonances for thin gold films: Surface plasmon resonances for thin Au films *Phys. Status Solidi A* **210** 2445–55
[22] Shukla S, Sharma N K and Sajal V 2015 Sensitivity enhancement of a surface plasmon resonance based fiber optic sensor using ZnO thin film: a theoretical study *Sensors and Actuators B: Chemical* **206** 463–70
[23] Masruroh, Maulana G A, Syarifuddin I M, Sukma F O R, Hanif M A, Saroja G, Tjahjanto R T and Santjojo D J D H 2025 Tuning Viscosity and Spin Time to Enhance the Thinnest rGO Film Coating in SPR Sensors *Plasmonics* **20** 6105–14
[24] Ekgasit S, Thammacharoen C and Knoll W 2004 Surface Plasmon Resonance Spectroscopy Based on Evanescent Field Treatment *Anal. Chem.* **76** 561–8.